

Impacts of climate change and variability on tropospheric ozone and its precursors

David Stevenson¹, Ruth Doherty¹, Michael Sanderson², Colin Johnson², Bill Collins² & Dick Derwent³

¹Institute for Atmospheric and Environmental Science, The University of Edinburgh

²Hadley Centre for Climate Prediction and Research, Met. Office, Exeter

³rdscientific, Newbury

Abstract

Two coupled climate-chemistry model experiments for the period 1990-2030 were conducted: one with a fixed climate and the other with a varying climate forced by the is92a scenario. By comparing results from these experiments we have attempted to identify changes and variations in physical climate that may have important influences upon tropospheric chemical composition. Climate variables considered include: temperature, humidity, convective mass fluxes, precipitation, and the large-scale circulation. Increases in humidity, directly related to increases in temperature, exert a major influence on the budgets of ozone and the hydroxyl radical: decreasing O₃ and increasing OH. Warming enhances decomposition of PAN, releasing NO_x, and increases the rate of methane oxidation. Surface warming enhances vegetation emissions of

isoprene, an important ozone precursor. In the changed climate, tropical convection generally reduces, but penetrates to higher levels. Over northern continents, convection tends to increase. These changes in convection affect both vertical mixing and lightning NO_x emissions. We find no global trend in lightning emissions, but significant changes in its distribution. Changes in precipitation and the large-scale circulation are less important for composition, at least in these experiments. Higher levels of the oxidants OH and H_2O_2 lead to increases in aerosol formation and concentrations. These results indicate that climate-chemistry feedbacks are dominantly negative (less O_3 , a shorter CH_4 lifetime, and more aerosol). The major mode of inter-annual variability in the is92a climate experiment is ENSO. This strongly modulates isoprene emissions from vegetation via tropical land surface temperatures. ENSO is also clearly the dominant source of variability in tropical column ozone, mainly through changes in the distribution of convection. The magnitude of inter-annual variability in ozone is comparable to the changes brought about by emissions and climate changes between the 1990s and 2020s, suggesting that it will be difficult to disentangle the different components of near-future changes.

1. Introduction

'When we try to pick out anything by itself, we find it hitched to everything else in the Universe' – John Muir (1838-1914)

Over recent years, several modelling studies (e.g., Stevenson et al., 1998; Hauglustaine and Brasseur, 2001; Prather et al., 2001, 2003; Gauss et al., 2003) have made estimates of future tropospheric composition. In these studies the main driver of change is the evolution of the magnitude and spatial distribution of anthropogenic trace gas emissions (e.g., Nakicenovic et al., 2000). There has also been an appreciation that future changes in physical climate may exert additional significant influences on composition, but modelling studies in this area have been less common. Several potentially important chemistry-climate feedbacks have been explored, such as those involving temperature, water vapour (Johnson et al., 1999, 2001; Stevenson et al., 2000; Shindell et al., 2001), precipitation (Grewe et al., 2001), stratosphere-troposphere exchange (Collins et al., 2003; Zeng and Pyle, 2003), and climate-driven changes in natural biogenic (Sanderson et al., 2003a) and lightning emissions (Toumi et al., 1996). A recent review of ozone-climate interactions discusses many of these (Isaksen et al., 2003). There have been even fewer studies of the impact of inter-annual climate variability on global tropospheric composition (e.g., Peters et al., 2001; Johnson et al., 2002; Warwick et al., 2002; Ziemke and Chandra,

2003), and little attempt to compare the mechanisms involved in these two overlapping areas.

In this paper, we present new results from a state-of-the-art coupled climate-chemistry model (HadAM3-STOCHEM), which has been applied to the time period 1990-2030. We analyse the results in terms of the effects of climate change and climate variability on composition, mainly focussing on tropospheric ozone and its precursors. We first document the relevant physical climate drivers in these experiments. We then show how these drivers affect important natural emissions sources in the model, change in-situ chemical processes, and hence modify concentrations and distributions of a variety of trace species. We separately look at the influences on composition of both long-term climate change and inter-annual climate variability. We then discuss the relative importance of the various climate-chemistry interactions included in our model results, whilst noting some potentially important missing processes not considered in this work.

2. Climate-Chemistry Model

The HadAM3-STOCHEM coupled climate-chemistry model (Sanderson et al., 2003a, b; Stevenson et al., 2004) was used to carry out the series of numerical experiments. The chemistry sub-model receives meteorological fields from the driving climate model, but chemical fields were not fed back into the radiation

scheme of the climate model in the experiments described here. The model couples emissions of isoprene from vegetation and lightning NO_x to meteorological variables. A brief description of the main model components follows.

2.1. Climate model: HadAM3

The Hadley Centre atmosphere-only climate model (HadAM3, Pope et al., 2000) is a general circulation model (GCM) describing the state of the atmosphere. Prescribed sea surface temperatures (SSTs) provide the lower boundary condition over the oceans. Over land, the MOSES2.2 surface exchange scheme is employed (Essery et al., 2001), together with a prescribed seasonal vegetation distribution. HadAM3 was run at standard climate resolution: 3.75° longitude x 2.5° latitude, with 19 vertical levels, concentrated towards the surface, but extending upwards to ~10 hPa. The model time-step was 30 minutes, with meteorological fields passed to STOCHEM every 3 hours.

2.2. Chemistry sub-model: STOCHEM

STOCHEM is a Lagrangian tropospheric chemistry-transport model, originally described by Collins et al. (1997), with subsequent major updates to chemistry (Collins et al., 1999), convective mixing (Collins et al., 2002), surface

deposition (Sanderson et al., 2003b), and vegetation emissions (Sanderson et al., 2003a). STOCHEM extends from the surface to ~100 hPa; this is approximately the level of the tropical tropopause, but is some way into the lower stratosphere at higher latitudes. Consequently, we mainly limit our discussion here to tropospheric composition. The climate model that drives STOCHEM extends to higher levels (~10 hPa), to improve the representation of the stratospheric circulation, and in particular stratosphere-troposphere exchange. The STOCHEM domain is divided into 50,000 equal mass air parcels, which are advected using winds from HadAM3, using a fourth order Runge-Kutta method. Every 1 hour advection time-step, winds are linearly interpolated to each parcel's position in the horizontal, and using cubic interpolation in the vertical. A random walk component is added to simulate horizontal and vertical diffusion. Following each advection step, air parcels are mapped to a latitude-longitude grid of dimensions $5^\circ \times 5^\circ$ with nine equally spaced vertical levels, of thickness ~100 hPa. Each grid-box contains, on average, two to three Lagrangian air parcels. To represent the deformation of air parcels, some inter-parcel mixing is implemented between air parcels within the same grid-box. Air parcel concentrations are brought towards the mean value for the grid-box. Turbulent mixing in the boundary layer is achieved by randomly re-assigning the vertical co-ordinates of air parcels over the depth of

the layer. Convective mixing is described fully in Collins et al. (2002), and utilizes 3-D convective mass fluxes.

Global trace gas emissions, by sector and species, follow the International Institute for Applied Systems Analysis (IIASA) 'Current Legislation' (CLE) scenario for 1990-2030, and are described in detail by Dentener et al. (2004). Stevenson et al. (2004) showed that this model configuration was able to successfully simulate many of the features of the recent ozone and methane observational records.

Vegetation emissions of isoprene are distributed using spatial vegetation fields from the GCM land surface scheme, and include a dependence upon temperature and photosynthetically available radiation, following the scheme described by Sanderson et al. (2003a).

Interactive lightning NO_x emissions are based on the parameterizations of Price et al. (1997). The total number of lightning flashes is calculated from the cloud height, using two different formulae for continental and maritime clouds. The proportions of inter-cloud and cloud-to-ground lightning are calculated from the cold cloud thickness using the formula of Price et al. (1997), and from the number of flashes the NO production may be calculated. Once produced, the NO is distributed in the vertical using the profiles of Pickering et al. (1998).

The chemical scheme is described by Collins et al. (1999), and includes 70 species that take part in 174 photochemical, gas-phase, and aqueous-phase reactions and equilibria. The mechanism describes the tropospheric chemistry of CH₄, CO (carbon monoxide), NO_x, O₃, and 11 non-methane hydrocarbons (NMHC). There is no specific representation of stratospheric chemistry in this model version. Several aqueous phase reactions and equilibria are included (see Stevenson et al., 2003); there is a simplified representation of heterogeneous reactions that convert NO_y to nitrate aerosol, with a fixed global rate constant. The chemical time-step is 5 minutes. The dry and wet deposition schemes are described in detail by Sanderson et al. (2003b) and Stevenson et al. (2003), respectively. To represent the influx of stratospheric O₃ to the top of the model domain, we use vertical wind fields at 100 hPa, coupled with an ozone climatology (Li and Shine, 1995). Similarly, we introduce an NO_y (total oxidized nitrogen) influx (as HNO₃), assuming a fixed mass ratio of N:O₃ of 1:1000 (Murphy and Fahey, 1994).

3. Numerical experiments

Two 40-year experiments were carried out, covering the period 1990-2030. In both experiments, the chemistry sub-model used the same CLE trace gas emission scenario, but the climate model was forced in two different ways. In the first experiment (A), the climate was driven by annually invariant SSTs and

sea-ice (the average over the AMIP time period 1978-1996: Taylor et al., 2000), and greenhouse gas concentrations used in the radiation scheme were fixed at 1990 levels. This experiment therefore examines only the effect of increasing trace gas emissions on tropospheric composition. The second experiment (B) used SSTs and sea-ice from an earlier run of the coupled ocean-atmosphere model HadCM3 (Johns et al., 2003), forced by the is92a scenario (Leggett et al., 1992) of greenhouse gases and aerosols, similar to the model simulation reported by Cox et al. (2000). Greenhouse gas concentrations in experiment (B) also followed the is92a scenario. Note that to be perfectly consistent we should have used SSTs and greenhouse gas concentrations from the CLE scenario and not the is92a scenario. However such data are not available. The is92a scenario represents a climate trajectory in the middle (in terms of global surface temperature change) of more recent (Cubasch et al., 2001) projections for the near future. Experiment (B) shows global tropospheric warming of ~ 1 K between the 1990s and 2020s, with larger changes over the continents and Polar Regions; a common pattern of future climate change amongst climate models (Cubasch et al., 2001). As such, it serves our purpose of assessing potential feedbacks between climate and chemistry.

4. Results

Firstly, we document changes in physical climate of potential importance for chemistry. Secondly, we present model-derived changes in natural emissions driven by some of these changes in physical climate. Thirdly, we show changes in the distribution of various chemical species; these are generated by a complex combination of climate-driven changes in physical processes, in-situ chemical reaction rates, and natural emissions. In general, to isolate the effects of mean climate change, we present results as decadal average differences, in order to reduce the noise introduced by inter-annual variability. We define ‘the impact of climate change between the 1990s and 2020s on field X’ as (where X = T, O₃, etc.):

$$\Delta X = (X(B, 2020s) - X(B, 1990s)) - (X(A, 2020s) - X(A, 1990s)) \quad (1)$$

This removes any effects of offsets in 1990s climate between (A) and (B), and also removes the effects of emissions growth over 1990-2030 for chemical species. Finally, to assess the importance of inter-annual variability of climate on tropospheric composition, correlation and EOF analyses were performed using experiment (B). The Niño-3 index which represents Central Pacific SSTs was constructed and EOF analysis performed to establish the dominant pattern and corresponding principal component time series of inter-annual variability in tropospheric column ozone.

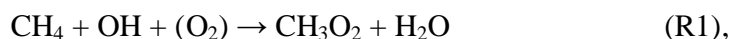
4.1 Changes in physical climate

4.1.1 Temperature

Figure 1a shows the zonal mean change in temperature (ΔT ; see definition above) due to climate change between the 1990s and 2020s decades.

Temperatures increase throughout the troposphere, with the largest increases in the tropical upper troposphere (UT) and in the high Northern latitude lower troposphere (LT). The Northern hemisphere (NH) shows more warming than the Southern hemisphere (SH). The lower stratosphere (LS) shows some cooling. Figure 1b shows the geographical distribution of the change in surface temperature, and indicates that the greatest warming is generally over land, with peaks of >2 K over S. America, Central Asia and the Arctic.

Several major reactions in the troposphere have strong temperature dependence, including the oxidation of CH_4 :



and the thermal decomposition of PAN (peroxyacetyl nitrate, $\text{CH}_3\text{COO}_2\text{NO}_2$):



Both reactions proceed more rapidly as temperature increases. Reaction (R1) is the main removal mechanism for methane, and also a major control on OH levels. PAN is the major NO_y reservoir species, and makes a significant

contribution to the long-range transport of reactive nitrogen, and hence promotes O₃ formation in remote regions.

4.1.2 Water vapour

Figure 2 shows the zonal mean change in water vapour (ΔQ) between the 1990s and 2020s due to climate change. The warmed troposphere holds more water – the absolute changes are largest in the warmest, wettest regions of the atmosphere, i.e., towards the surface and the equator. Because the NH shows more warming, it also displays larger increases in water vapour compared to the SH. In percentage terms, the changes in water vapour are largest in the UT (not shown). As H₂O is the dominant precursor of the highly reactive hydroxyl radical (OH), via its reaction with excited oxygen atoms:



we expect this change in physical climate to have an important influence on tropospheric chemistry. Reaction (R3) is also the main sink for tropospheric O₃.

4.1.3 Convection

Figure 3a shows the zonal mean change in convective updraught strength between the 1990s and 2020s due to climate change. This shows increases in shallow convection in the tropics and at high Northern latitudes, but decreases in mid-latitudes. In the mid-troposphere (MT), convective updraughts are

generally reduced, particularly in the tropics. However, perhaps the most important factor for tropospheric chemistry is an increase in the strength of the very deepest tropical convection; this can be seen more clearly in Figure 3b, which shows the change in updraught strength in the uppermost STOCHEM level.

Convection has a marked impact on several species; perhaps most importantly, increased convection tends to reduce column O_3 , except over polluted regions (Doherty et al., 2004). Increased convection reduces the lifetime of the majority of O_3 molecules (see section 4.4.3). Convective parameters are also used in the model's interactive lightning scheme, thus changes in convection also effect the location and magnitude of lightning NO_x emissions. Other models exhibit quite different sensitivities in composition to convection (e.g., Lelieveld and Crutzen, 1994; Lawrence et al., 2003).

4.1.4 Precipitation

Figure 4 shows the change in total precipitation (convective plus dynamic; rain and snow) between the 1990s and 2020s due to climate change. Changes in tropical convective rainfall dominate the picture with a strengthening of the inter-tropical and South Pacific convergence zones (ITCZ and SPCZ respectively) and hence monsoonal rainfall (linked to the strength and northward movement of the ITCZ). This results in increased rainfall over the

Pacific and Asian monsoon regions, but decreased rainfall over Indonesia, the Indian Ocean, and Central and S. America. The increases coincide with areas of increases in deep convection (Figure 3b), whilst decreased MT updraughts may explain the decreases in precipitation seen over some tropical land regions.

Changes in precipitation may be important for soluble species whose main sink is via wet deposition, e.g., nitric acid (HNO_3) and hydrogen peroxide (H_2O_2).

4.1.5 Large-scale transport

Collins et al. (2003), using a version of STOCHEM coupled to the HadAM4 climate model (these versions have higher vertical resolution than those used here), showed that the net influx of ozone from the stratosphere to the troposphere increased by 37% between the 1990s and 2090s, with the climate forced by the A1FI scenario (Nakicenovic et al., 2000). Under this ‘fossil fuel intensive’ scenario, surface temperatures rise by ~5K by 2100. This can be compared to a more moderate rise of ~1K by 2030 in the experiments described here. The calculated stratospheric influx of ozone shows no significant trend in either experiment (A) or (B) (Table 1).

4.2 Climate-driven changes in emission

4.2.1 Isoprene from vegetation

The model includes interactive emissions of isoprene from vegetation – the increases in land surface temperature (Figure 1b) result in an increase in C₅H₈ emission (Figure 5). Between the 1990s and 2020s, isoprene emissions increase by ~9% in experiment (B), most notably over S. America (the largest isoprene emitting region). Increases in isoprene can result in either increased O₃ production (in areas of sufficiently high NO_x), or O₃ destruction (in areas of low NO_x). Sanderson et al. (2003a) previously showed that increases in C₅H₈ emission generally led to increased O₃ levels.

Other climate-sensitive biospheric sources (such as wetland CH₄, soil NO_x, biomass burning, and oceanic emissions) are not linked interactively to climate in these experiments, but are prescribed as monthly varying, annually invariant fields.

4.2.2 Lightning NO_x

The interactive lightning NO_x scheme in STOCHEM links emissions to convective cloud parameters. Emissions have been scaled to give a global annual total of c.7 Tg(N) yr⁻¹ in the 1990s. There is no significant trend in the global magnitude of lightning NO_x emissions in either experiment, but some

shifts in the vertical and horizontal distribution of lightning with climate change (Figure 6). The tropics show less in total, with reductions over S. America, W. Africa, and India, but increases over S.E. Asia (Figure 6b,c), reflecting the changes in convective precipitation (Figure 4). However, the tropics generally show more lightning at higher altitude (Figure 6a,c); these changes reflect reduced, but deeper tropical convection, as shown in Figure 3a. The areas of increased deep convection over land (Figure 3b) are the areas that show the largest increases in UT lightning (Figure 6c). The NH mid-latitudes, especially N. America and E. Asia show increases lightning, roughly balancing the tropical reduction.

4.3 Climate-driven changes in tropospheric composition

Figure 7a-c shows changes in the distributions of the key reactive nitrogen species induced by changes in climate. PAN (Figure 7a) shows decreases throughout the troposphere, due to the strong temperature dependence of its decomposition (reaction R2). The decreases are strongest in high northern latitudes, where PAN concentrations are highest, and where the LT warming is greatest (Figure 1). Only in the cooling LS do PAN concentrations increase. Over the whole model domain, PAN concentrations fall by 7% in response to climate change.

HNO₃ (Figure 7b) shows modest increases (up 1.5% globally), partly due to increased levels of OH (Figure 7e: see below) and enhanced conversion of NO_x. Changes in wet removal, through changes in precipitation (Figure 4) do not appear to be very important.

Increases in NO_x at high northern latitudes (Figure 7c) are mainly due to PAN decomposition (Figure 7a). Changes in the tropics and mid-latitudes are related to changes in lightning emissions (Figure 6), but are also less directly to convective mixing (Figure 3). Less tropical convection leads to higher NO_x concentrations in the LT at the expense of the UT; the opposite appears to be the case over NH mid-latitude land.

Climate change tends to reduce ozone throughout the troposphere (Figure 7d), by about 3.6% (Table 1). This is despite a general increase in ozone chemical production (Figure 8a; Table 1). Only the regions of the tropics with lightning NO_x reductions show significant decreases in production. The reason for this apparent contradiction is a parallel increase in ozone chemical destruction (Figure 8b; Table 1), mainly due to increases in water vapour (Figure 2) and hence the ozone destroying reaction (R3). Net chemical production (Figure 8c; Table 1) shows decreases throughout most of the MT and UT, particularly in the tropics; only in the LT is there an increase, mainly fuelled by higher isoprene emissions (Figure 5). In the background atmosphere, ozone lifetime

increases strongly with altitude, mainly due to the reduction in temperature and hence water vapour. This means that changes in net ozone production in the UT have a larger influence on global ozone burden. A further reason for the decline in ozone burden is the reduction in the ozone lifetime almost everywhere (Figure 8d; Table 1), typically by 5-10% in the NH. Even if net chemical production of ozone were to remain constant, a reduction in lifetime would lower concentrations.

Partly mirroring the decline in ozone is an increase in OH (Figure 7e), also brought about via reaction (R3), although this is only part of the explanation. Changes in NO_x also influence OH, as do changes in temperature. Warming increases the flux through methane oxidation (reaction R1), which contributes to the reduction in OH towards the surface in the SH tropics.

Elevated OH in the NH leads to faster hydrocarbon oxidation, which, together with the higher levels of isoprene, raises the levels of CO (up 2% globally) and other oxidation products such as formaldehyde (HCHO: up 3% globally). The hydroperoxy radical (HO_2) also shows increases of 3%, and hydrogen peroxide (H_2O_2) increases by 5%. These rises in OH and H_2O_2 enhance aerosol formation from precursors such as SO_2 . Figure 7f shows the increase in sulphate aerosol due to climate change; this represents a global increase of 4%.

To place these climate change induced changes in tropospheric composition in context, Figure 9 shows the calculated changes in column and surface ozone between the 1990s and 2020s due to only emissions changes (Figure 9a and b), and due to climate change (Figure 9c and d). The emissions only results are discussed in detail by Dentener et al. (2004). TC ozone changes due to increasing emissions in the 2020s decade relative to the 1990s decade are shown in Figure 9a. In the NH, TC ozone increases by 1-3 DU and up to 5.5 DU over India, S.E. Asia and outflow regions over the N. Pacific. Surface ozone shows similar features, with additional strong increases over the N. Atlantic, related to increases in ship emissions (Derwent et al., 2004). Changes in TC ozone due to climate change alone between the 1990s and 2020s are shown in Figure 9c. This figure complements Figure 7d, and Table 1, which shows a 3.6% reduction in tropospheric ozone burden due to climate change over the time period. Figure 9d shows changes in surface O₃ due to climate change. Ozone reductions over the tropical Pacific can be understood in terms of increases in water vapour and ozone destruction. Increases in surface ozone over S. America, C. Africa, and parts of S.E. Asia can be related to increased isoprene emissions (Figure 5). Increases in lightning NO_x over S.E. Asia (Figure 6) also contribute to the ozone changes. However, for many of the features, a complex combination of factors is probably important.

4.4 Inter-annual climate variability and tropospheric chemistry

The strongest natural fluctuation of climate on inter-annual timescales is ENSO. It originates in the tropical Pacific but affects regional climate conditions globally. Studies speculate but disagree on whether climate change may bring about a long-term mean shift in Pacific sea-surface temperatures towards a more El Niño or La Niña like mean state. Global climate models reproduce ENSO and its teleconnections to a certain extent. Besides elevated tropical (and global) temperatures, El Niño activity is associated with an eastward shift in convection across the tropical Pacific, resulting from changes in the Walker circulation, which in turn brings about teleconnections to global climate (e.g., Ropelewski and Halpert, 1986). HadCM3 generates a rather too regular cycle of 3-4 years (Collins et al., 2001); in addition the overall warming in our case (Figure 1b) has some El Niño-like features, as has been noted in an earlier HadCM3 study (Cox et al., 2004).

4.4.1 Physical climate variability

In this study, the Niño-3 index (Figure 10) shows strongly negative SST anomalies which indicate La Niña episodes in the early part of the simulation with some weaker episodes in the later stages of the experiment. Generally, however there is a tendency towards strong positive Niño-3 anomalies (Figure 10) or El Niño episodes for most of the model simulation.

4.4.2 Inter-annual variability and natural emissions

ENSO-induced climate variability has a strong influence on global isoprene emissions in our coupled scheme (Figure 10a). We found a correlation coefficient of 0.86 between Niño-3 and isoprene emissions. S. America is the largest regional source of isoprene emissions (see section 4.2.1), followed by N. Africa, S. Asia, and S. Africa. As discussed above, El Niño events in the tropical Pacific bring about regional variations in temperature and precipitation. S. America experiences higher temperatures and hence higher isoprene emissions. Temperatures are also generally elevated in S. Africa during El Niño conditions. Inter-annual variations in global isoprene emissions represent about 25% of the total change in global isoprene emissions due to warming between the 1990s and 2020s decades (discussed in section 4.2.1.)

There is a much weaker relationship between ENSO and global lightning NO_x emissions ($r=-0.4$, significant at the 0.01 level, Figure 10b). Lightning emissions are strongest over the tropics; S. America and S. Asia exhibit a negative relationship between lightning NO_x and Niño-3, whereas N. Africa shows a positive relationship. The former two regions experience drier conditions and therefore less convective activity during El Niño events, and also show less lightning due to climate change (Figure 6b and c).

4.4.3 Inter-annual variability in ozone

On inter-annual timescales, ENSO is the dominant mode of variability in tropospheric column (TC) ozone (Figure 11). The first EOF pattern shows a strong ENSO-like signature with reduced TC ozone in the central and eastern tropical Pacific and enhanced TC ozone over the western Pacific. The first EOF PC1 time series correlates extremely highly with the Niño-3 index ($r=0.84$, Figure 11b), and a high percentage variance (31%) of the inter-annual signal is explained by this first EOF, confirming that ENSO behaviour dominates the inter-annual signal of ozone variability.

Over the Central and Eastern tropical Pacific there is increased convective activity during El Niño events. Surface air in this clean region, which is relatively ozone-poor, experiences more upwards mixing due to the enhanced convection; this tends to lengthen the ozone lifetime for this air. However, at the same time, relatively ozone-rich UT air experiences more down-mixing, tending to reduce the lifetime of these ozone molecules. Because ozone typically increases with altitude, over the tropospheric column, we find that the latter process dominates. Thus enhanced convective mixing reduces TC ozone, by typically 1-2 DU (and up to 2-3 DU, Figure 11a) in the central and eastern Pacific. Generally the converse applies over the western Pacific and TC ozone increases typically by 0.5 DU (up to 1-2 DU, Figure 11a). The pattern of ozone

change is more extended than the ENSO-related convective changes, demonstrating that the signal experiences some transport away from the anomaly source regions.

5. Discussion and Conclusions

These results give some indications of the relative importance of different climate-chemistry feedbacks, which are summarized in Table 2. Increases in water vapour, associated with tropospheric warming, lead to enhanced O₃ destruction (reaction R3), a shorter O₃ lifetime, and consequently reduce O₃ concentrations throughout most of the troposphere. Apparently less important influences stem from enhanced isoprene emissions from vegetation, which locally increase LT ozone over some tropical land masses; and changes in convection, which affect vertical mixing and lightning, with some regional affects on NO_x and ozone. The results also indicate no change in stratospheric input of O₃ to the troposphere, whereas other studies (Collins et al., 2003; Zeng and Pyle, 2003) suggest important increases in this source of ozone. Further work is clearly needed to reach a consensus on this issue.

The NO_x distribution is strongly affected at high northern latitudes by increased thermal decomposition of PAN (reaction R2), promoted by warming. At the same time as destroying ozone, reaction (R3) generates OH. However, warming, particularly in the tropical LT, increases methane oxidation (R1),

tending to deplete OH. Changes in the NO_x distribution also affect OH, but overall, warming appears to increase levels of OH, particularly in the NH. One consequence of this is increased oxidation of hydrocarbons, and higher levels of CO, HO₂, HCHO and H₂O₂; another is increased aerosol formation. One consistent finding of these results is that climate-chemistry feedbacks are dominantly negative (less O₃, a shorter CH₄ lifetime, and more aerosols). The dominant mode of inter-annual climate variability (ENSO) also appears to be the major mode of chemical variability, and the important linking process is convective mixing. Natural variability in tropical TC ozone (Figure 11a) is comparable in magnitude to changes caused by climate change between the 1990s and 2020s (Figure 9c); in addition both processes generate effects within a factor of two of the ozone changes expected from emissions changes over the same time period (Figure 9a). This illustrates the importance of considering natural variability and climate change, as well as emissions changes, in future projections of chemical composition.

We must end this paper on several notes of caution. As referred to earlier there are a number of potentially important missing processes. The results presented here are representative of just one model, and it remains to be seen whether other models exhibit feedback mechanisms of similar magnitude or even feedbacks with the same sign. Future water vapour concentrations are of prime

importance for chemistry, but have many uncertainties. Model water vapour feedbacks have been the subject of several studies which use seasonal variations to calculate the magnitudes of the feedback (e.g., Slingo et al, 2000; Stocker et al., 2001). These studies show a broad agreement in modelled and measured feedbacks. Forster and Collins (2004) compare water vapour feedbacks associated with the Mt. Pinatubo volcanic eruption to compare modelled and measured humidities. While the measured global feedback parameter was in the range of model results, differences between modeled and observed water vapour response in the UT were found. Our model also lacks many potentially important processes, such as linkages between heterogeneous chemistry, wetland CH₄, biomass burning, oceanic and soil emissions and climate. Many other important aspects of the model, such as its simulation of ENSO behaviour, and its convection scheme are quite poorly understood. In addition, we have considered just a single future climate scenario.

Acknowledgements

DSS thanks the Environment Agency and Natural Environment Research Council for fellowship funding (P4-F02, NER/J/S/2000/00840). RMD thanks NERC for UTLS-O₃ funding (NER/T/S/2000/01041). MJS, WJC and CEJ acknowledge funding from the Government Meteorological Research programme and DEFRA through contract CPEA7.

References

- Collins, M., S.F.B. Tett, and C. Cooper, The internal climate variability of HadCM3, a version of the Hadley Centre coupled model without flux adjustments, *Climate Dyn.*, 61-81, 2001.
- Collins, W. J., D. S. Stevenson, C. E. Johnson, and R. G. Derwent, Tropospheric ozone in a global-scale three-dimensional Lagrangian model and its response to NO_x emission controls, *J. Atmos. Chem.*, 26, 223-274, 1997.
- Collins, W. J., D. S. Stevenson, C. E. Johnson, and R. G. Derwent, The role of convection in determining the budget of odd hydrogen in the upper troposphere, *J. Geophys. Res.*, 104, D21, 26927-26941, 1999.
- Collins, W. J., R. G. Derwent, C. E. Johnson, and D. S. Stevenson, A comparison of two schemes for the convective transport of chemical species in a Lagrangian global chemistry model, *Q. J. R. Meteorol. Soc.*, 128, 991-1009, 2002.
- Collins, W. J., R. G. Derwent, B. Garnier, C. E. Johnson, M. G. Sanderson and D. S. Stevenson, The effect of stratosphere-troposphere exchange on the future tropospheric ozone trend, *J. Geophys. Res.*, 108 (D12), doi: 10.1029/2002JD002617, 2003.

- Cox P.M., Betts R.A., Jones C.D., Spall S.A. and Totterdell I.J., Amazonian forest dieback under climate-carbon cycle projections for the 21st Century, *Nature*, 408, 184-187, 2000.
- Cox, P.M., R.A. Betts, M. Collins, P.Harris, C. Huntingford and C. D. Jones, Amazon dieback under climate-carbon cycle projections for the 21st century, *Theoretical and Applied Climatology*, 78(1-3), 137-156, 2004.
- Cubasch, U., G.A. Meehl, G.J. Boer, R.J. Stouffer, M. Dix, A. Noda, C.A. Senior, S. Raper, and K.S. Yap (2001) Projections of future climate change, In: *Climate Change 2001: The Scientific Basis*, Contribution of WG1 to the Third Assessment report of the IPCC, Eds. Houghton, J.T., et al., Cambridge University Press, England, 2001.
- Dentener, F.D., D.S. Stevenson, J. Cofala, R. Mechler, M. Amann, P. Bergamaschi, F. Raes, and R.G. Derwent, Tropospheric methane and ozone in the period 1990-2030: CTM calculations on the role of air pollutant and methane emissions controls, in preparation for *Atmospheric Chemistry and Physics*, 2004.
- Derwent, R.G, D.S. Stevenson, R.M. Doherty, W.J. Collins, M.G. Sanderson, C.E. Johnson, J. Cofala, R. Mechler, M. Amann, and F.J. Dentener, The contribution from ship emissions to air quality and acid deposition in Europe, submitted to *Ambio*, 2004.

- Doherty, R.M., D.S. Stevenson, C.E. Johnson, M.G. Sanderson, and W.J. Collins, Tropical Convection, ENSO and their influence on tropospheric ozone, in preparation for *Atmospheric Chemistry and Physics*, 2004.
- Essery, R., M. Best, and P. Cox, MOSES2.2 Technical Documentation, Hadley Centre Technical Note No. 30 (<http://www.metoffice.com/research/hadleycentre/pubs/HCTN>), Met. Office, U.K., 2001.
- Forster, P.M.D.F, and M. Collins, Quantifying the water vapour feedback associated with post-Pinatubo global cooling, *Climate Dyn.*, 23, 207-214, 2004.
- Gauss, M., et al., Radiative forcing in the 21st century due to ozone changes in the troposphere and the lower stratosphere, *J. Geophys. Res.*, 108 (D9), doi: 10.1029/2002JD002624, 2003.
- Grewe, V., M. Dameris, R. Hein, R. Sausen, and B. Steil (2001) Future changes of the atmospheric composition and the impact of climate change, *Tellus*, 53B, 103-121.
- Hauglustaine, D., and G.P. Brasseur, Evolution of tropospheric ozone under anthropogenic activities and associated radiative forcing of climate, *J. Geophys. Res.*, 106, 32337-32360, 2001.

- Isaksen, I.S.A., et al., Ozone-climate interactions, Air pollution report no.81 (EUR 20623), European Commission, Brussels, pp.143, 2003.
- Johns, T.C., J. M. Gregory, W. J. Ingram, C. E. Johnson, A. Jones, J. A. Lowe, J. F. B. Mitchell, D. L. Roberts, D. M. H. Sexton, D. S. Stevenson, S. F. B. Tett, and M. J. Woodage, Anthropogenic climate change for 1860 to 2100 simulated with the HadCM3 model under updated emissions scenarios, *Clim. Dyn.*, 20, 583-612, DOI 10.1007/s00382-002-0296-y, 2003.
- Johnson, C. E., W. J. Collins, D. S. Stevenson, and R. G. Derwent, The relative roles of climate and emissions changes on future oxidant concentrations, *J. Geophys. Res.* v.104, D15, 18631-18645, 1999.
- Johnson, C. E., D. S. Stevenson, W. J. Collins, and R. G. Derwent, Role of climate feedback on methane and ozone studied with a coupled Ocean-Atmosphere-Chemistry model, *Geophys. Res. Lett.* 28, 1723-1726, 2001.
- Johnson, C. E., D. S. Stevenson, W. J. Collins, and R. G. Derwent, Interannual variability in methane growth rate simulated with a coupled Ocean-Atmosphere-Chemistry model, *Geophys. Res. Lett.* 29(19), 1903, doi:10.1029/2002GL015269, 2002.
- Lawrence, M. G., R. von Kuhlmann, M. Salzmann, and P. J. Rasch, The balance of effects of deep convective mixing on tropospheric ozone, *Geophys. Res. Lett.*, 30(18), 1940, doi: 10.1029/2003GL017644, 2003.

- Leggett, J., W.J. Pepper, and R.J. Swart, Emissions scenarios for the IPCC: an update, In: Climate Change 1992, The supplementary report to the IPCC scientific assessment, Cambridge University Press, UK, pp.200, 2002.
- Lelieveld, J., and P. J. Crutzen, Role of Deep Cloud Convection in the Ozone Budget of the Troposphere, *Science*, 264, 1759-1761, 1994.
- Li, D., and K. P. Shine, A 4-dimensional ozone climatology for UGAMP models, UGAMP internal report, University of Reading, UK, 1995.
- Murphy, D. M., and D. W. Fahey, An estimate of the flux of stratospheric reactive nitrogen and ozone into the troposphere, *J. Geophys. Res.*, 99, 5325-5332, 1994.
- Nakicenovic, N., et al., IPCC Special Report on Emissions Scenarios, Cambridge University Press, Cambridge, UK, 570 pp., 2000.
- Peters, W., M. Krol, F.J. Dentener, and J. Lelieveld, Identification of an El Niño-Southern Oscillation signal in a multiyear global simulation of tropospheric ozone, *J. Geophys. Res.*, 106, (D10), 10389-10402, 2001.
- Pickering K.E., Y. Wang, W.-K. Tao, C. Price, and J.-F. Muller, Vertical distributions of lightning NO_x for use in regional and global chemical transport models, *J. Geophys. Res.*, 103, 31203-31216, 1998.

- Pope, V. D., M. L. Gallani, P. R. Rowntree, and R. A. Stratton, The impact of new physical parametrizations in the Hadley Centre climate model: HadAM3, *Clim. Dyn.*, 16, 123-146, 2000.
- Prather, M., D. Ehhalt, et al., Atmospheric Chemistry and Greenhouse Gases, In: *Climate Change 2001: The Scientific Basis*, Contribution of WG1 to the Third Assessment report of the IPCC, Eds. Houghton, J.T., et al., Cambridge University Press, England, 2001.
- Prather, M., M. Gauss, T.K. Berntsen, I. Isaksen, J. Sundet, I. Bey, G. Brasseur, F. Dentener, R. Derwent, D.S. Stevenson, L. Grenfell, D. Hauglustaine, L.W. Horowitz, D. Jacob, L.J. Mickley, M.G. Lawrence, R.v. Kuhlman, J.-F. Muller, G. Pitari, H. Rogers, M. Johnson, J.A. Pyle, K.S. Law, M.v. Weele, and O. Wild, Fresh air in the 21st century, *Geophys. Res. Lett.*, 30 (2), 72-72-4, 2003.
- Price, C., J. Penner, and M. Prather, NO_x from lightning 1. Global distribution based on lightning physics, *J. Geophys. Res.*, 102, 5929-5941, 1997.
- Ropelewski, C.F. and M.S. Halpert, Global and regional scale precipitation patterns associated with the El Niño/Southern Oscillation. *Mon. Weather. Rev.*, 115,1606-1626, (1987)
- Sanderson, M. G., C. D. Jones, W. J. Collins, C. E. Johnson, and R. G. Derwent, Effect of climate change on isoprene emissions and surface ozone

- levels, *Geophys. Res. Lett.*, 30(18), 1936, doi:10.1029/2003GL017642, 2003a.
- Sanderson, M. G., W. J. Collins, R. G. Derwent, and C. E. Johnson, Simulation of global hydrogen levels using a Lagrangian three-dimensional model, *J. Atmos. Chem.*, 46, 15-28, 2003b.
- Shindell, D. T., J. L. Grenfell, D. Rind, V. Grewe, and C. Price, Chemistry-climate interactions in the Goddard Institute for Space Studies general circulation model 1. tropospheric chemistry model description and evaluation, *J. Geophys. Res.*, 106, 8047-8075, 2001.
- Slingo, A., J.A. Pamment, R.P. Allen, and P.S. Wilson, Water vapour feedbacks in the ECMWF re-analyses and Hadley Centre climate model, *J. Climate*, 13, 3080-3098, 2000.
- Stevenson, D. S., C. E. Johnson, W. J. Collins, R. G. Derwent, K. P. Shine, and J. M. Edwards, Evolution of tropospheric ozone radiative forcing, *Geophys. Res. Lett.* 25, 3819-3822, 1998.
- Stevenson, D. S., C. E. Johnson, W. J. Collins, R. G. Derwent, and J. M. Edwards, Future tropospheric ozone radiative forcing and methane turnover - the impact of climate change, *Geophys. Res. Lett.* 27, 2073-2076, 2000.

- Stevenson, D. S., C. E. Johnson, E. J. Highwood, V. Gauci, W. J. Collins and R. G. Derwent, Atmospheric Impact of the 1783-84 Laki eruption: Part I Chemistry modelling, *Atmos. Chem. Phys.* 3, 487-507, 2003.
- Stevenson, D. S., R. M. Doherty, M. G. Sanderson, W. J. Collins, C. E. Johnson, and R. G. Derwent, Radiative forcing from aircraft NO_x emissions: mechanisms and seasonal dependence, *J. Geophys. Res.*, 109, D17307, doi:10.1029/2004JD004759, 2004.
- Stocker, T.F., et al., Physical climate processes and feedbacks, In: *Climate Change 2001: The Scientific Basis*, Contribution of WG1 to the Third Assessment report of the IPCC, Eds. Houghton, J.T., et al., Cambridge University Press, England, 2001.
- Taylor, K. E., D. Williamson, and F. Zwiers, The sea surface temperature and sea-ice concentration boundary conditions for AMIP II simulations, PCMDI Report No. 60 (<http://www-pcmdi.llnl.gov/pcmdi/pubs/ab60.html>), Program for Climate Model Diagnosis and Intercomparison, Lawrence Livermore National Laboratory, Livermore, California, 25 pp., 2000.
- Toumi, R., J. D. Haigh, and K. S. Law, A tropospheric ozone-lightning climate feedback, *Geophys. Res. Lett.*, 23, 1037-1040, 1996.

- Warwick, N. J., S. Bekki, K. S. Law, E. G. Nisbet, and J. A. Pyle, The impact of meteorology on the interannual growth rate of atmospheric methane, *Geophys. Res. Lett.*, 29(20), 1947, doi:10.1029/2002GL015282, 2002.
- Zeng, G., and J. A. Pyle, Changes in tropospheric ozone between 2000 and 2100 modeled in a chemistry-climate model, *Geophys. Res. Lett.*, 30(7), 1392, doi:10.1029/2002GL016708, 2003.
- Ziemke, J. R. and S. Chandra, La Niña and El Niño-induced variabilities of ozone in the tropical lower atmosphere during 1970-2001, *Geophys. Res. Lett.*, 30(3), 1142, doi:10.1029/2002GL016387, 2003.

Table 1 The ozone budget of the troposphere (defined as the region where $O_3 < 150$ ppbv) for the 1990s. Also shown is the percentage change by the 2020s due to emissions changes (i.e. just using results from experiment A), and the change by the 2020s due to climate change (following equation 1).

Budget term (Tg(O₃) yr⁻¹)	1990s (Expt A)	% change due to emissions by 2020s	% change due to climate change by 2020s
NO+HO ₂	3380	+4.5	+1.7
NO+CH ₃ O ₂	882	+17.7	+0.1
NO+RO ₂	715	+6.7	+4.1
Total Chem Prod	4977	+7.1	+1.8
O ₁ D+H ₂ O	2372	+8.2	+3.6
O ₃ +HO ₂	1237	+5.0	+0.5
O ₃ +OH	486	+6.4	+0.4
O ₃ +HCs	125	+2.2	+9.3
O ₃ other loss	230	+6.5	+1.2
Total Chem Loss	4450	+6.9	+2.4
Net Chem Prod	+527	+9.3	-3.8
Dry Deposition	939	+4.5	-2.0
Strat influx	415	+2.1	-0.5
O ₃ burden (Tg)	275	+4.2	-3.6
O ₃ lifetime (days)	18.4	-2.2	-4.3

Table 2 Summary of some important climate-chemistry feedbacks (not all of which are included in this study) and an indication of the impact of the feedback on composition. Where no comment is made, the impact is unknown.

Feedback	Included in this model study?	Impact of climate change
<i>Temperature-related</i>		
<i>T-dependent reactions</i>		
PAN decomposition	Y	PAN ↓ NO _x ↑
CH ₄ oxidation	Y	CH ₄ ↓ OH ↓ HO ₂ ↑
Other reactions	Y	
<i>T-dependent emissions</i>		
Vegetation C ₅ H ₈	Y	C ₅ H ₈ ↑ O ₃ ↑
Wetland CH ₄	N	
Anthropogenic emissions	N	
<i>Water vapour-related</i>		
O ¹ D + H ₂ O	Y	O ₃ ↓ OH ↑
Aqueous-phase chemistry	Y	
Heterogeneous chemistry	Y	
	(but no link to climate)	
<i>Circulation-related</i>		
<i>Convection</i>		
Vertical mixing	Y	Highly variable
Lightning	Y	Highly variable impacts on NO _x
<i>Strat-trop exchange</i>		
Stratospheric O ₃ input	Y	Other studies show O ₃ ↑
<i>Precipitation-related</i>		
Washout	Y	Highly variable
<i>Stratosphere-related</i>		
Changes in O ₃ and UV	N	

Figure Captions

Figure 1. (a) Zonal mean change in temperature (K) between the 1990s and 2020s due to climate change; (b) surface temperature difference (K) for the same time period.

Figure 2. Zonal mean change in humidity (ppm by mass) due to climate change between the 1990s and 2020s.

Figure 3 (a) Zonal mean change in convective updraught strength (mPa s^{-1}) due to climate change between the 1990s and 2020s; (b) change in convective updraught strength for the deepest convection (at ~ 150 hPa) for the same time period.

Figure 4 Change in total precipitation ($\text{mg m}^{-2} \text{s}^{-1}$) due to climate change between the 1990s and 2020s.

Figure 5 Change in isoprene emissions ($\text{Tg}(\text{C}_5\text{H}_8) \text{ yr}^{-1}$) due to climate change between the 1990s and 2020s.

Figure 6 Change in lightning NO_x emissions ($\text{Gg}(\text{N}) \text{ yr}^{-1}$) due to climate change between the 1990s and 2020s: (a) Zonal mean; (b) Column total; (c) 150 hPa level.

Figure 7 Zonal mean changes due to climate change between the 1990s and the 2020s: (a) PAN (pptv); (b) HNO_3 (pptv); (c) NO_x (pptv); (d) O_3 (ppbv); (e) OH (ppqv); (f) SO_4 (pptv).

Figure 8 Zonal mean change, due to climate change between the 1990s and 2020s, in (a) O₃ chemical production; (b) O₃ chemical destruction; (c) O₃ net chemical production; (d) O₃ lifetime.

Figure 9 Change in tropospheric column O₃ (a, c) and surface O₃ (b, d) between the 1990s and 2020s, due to emissions (a, b); and climate change (c, d).

Figure 10 Niño-3 index and: (a) C₅H₈ emissions variability; (b) Lightning NO_x emissions variability.

Figure 11 (a) First EOF for column O₃, over the full length of experiment (B); (b) First principal component and the Niño-3 index, demonstrating that ENSO is the major mode of variability in total tropospheric column ozone.

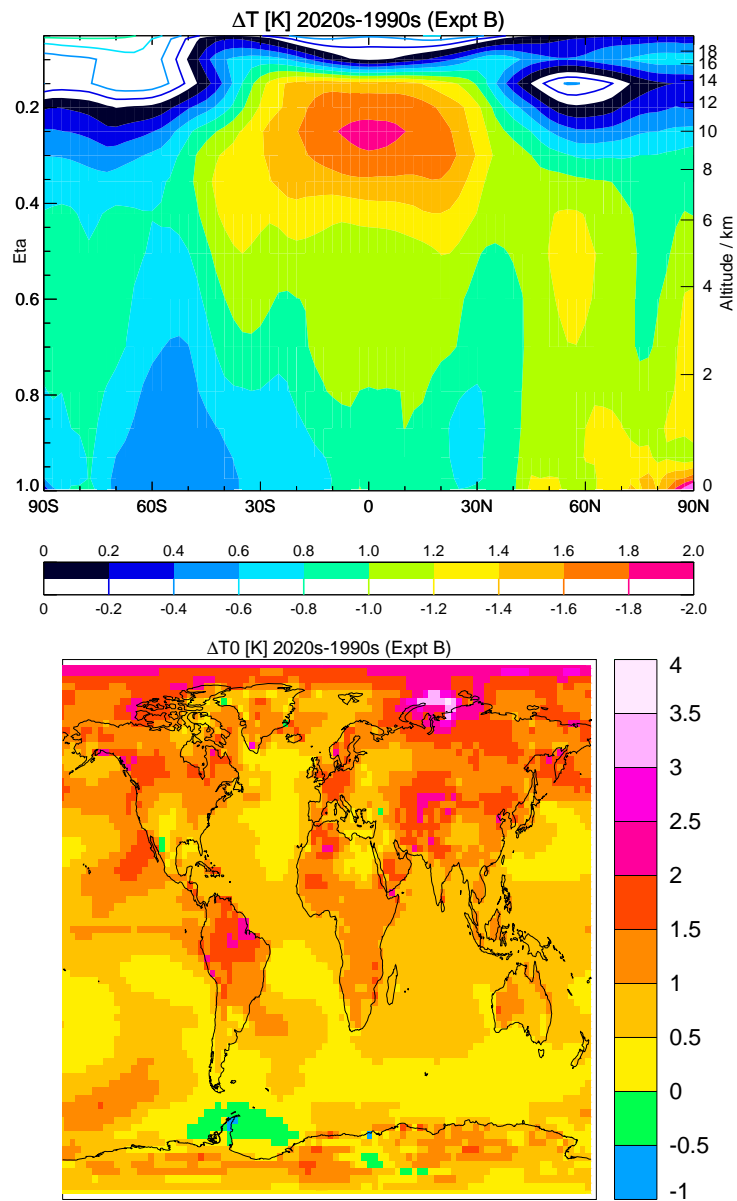


Figure 1. (a) Zonal mean change in temperature (K) between the 1990s and 2020s due to climate change; (b) surface temperature difference (K) for the same time period.

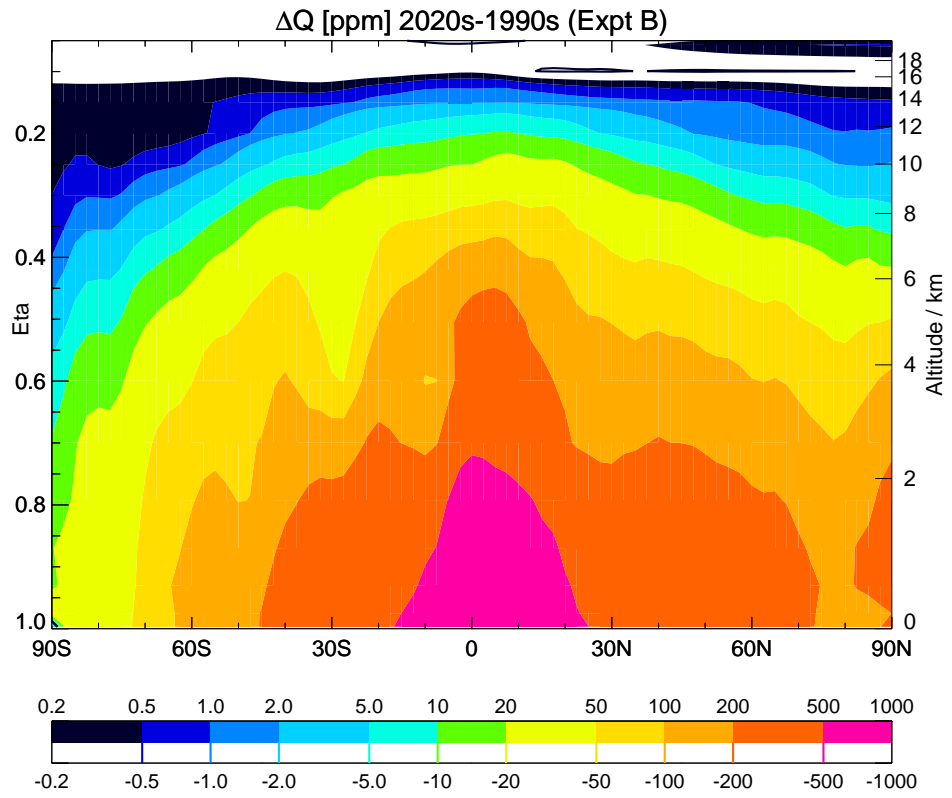


Figure 2. Zonal mean change in humidity (ppm by mass) due to climate change between the 1990s and 2020s.

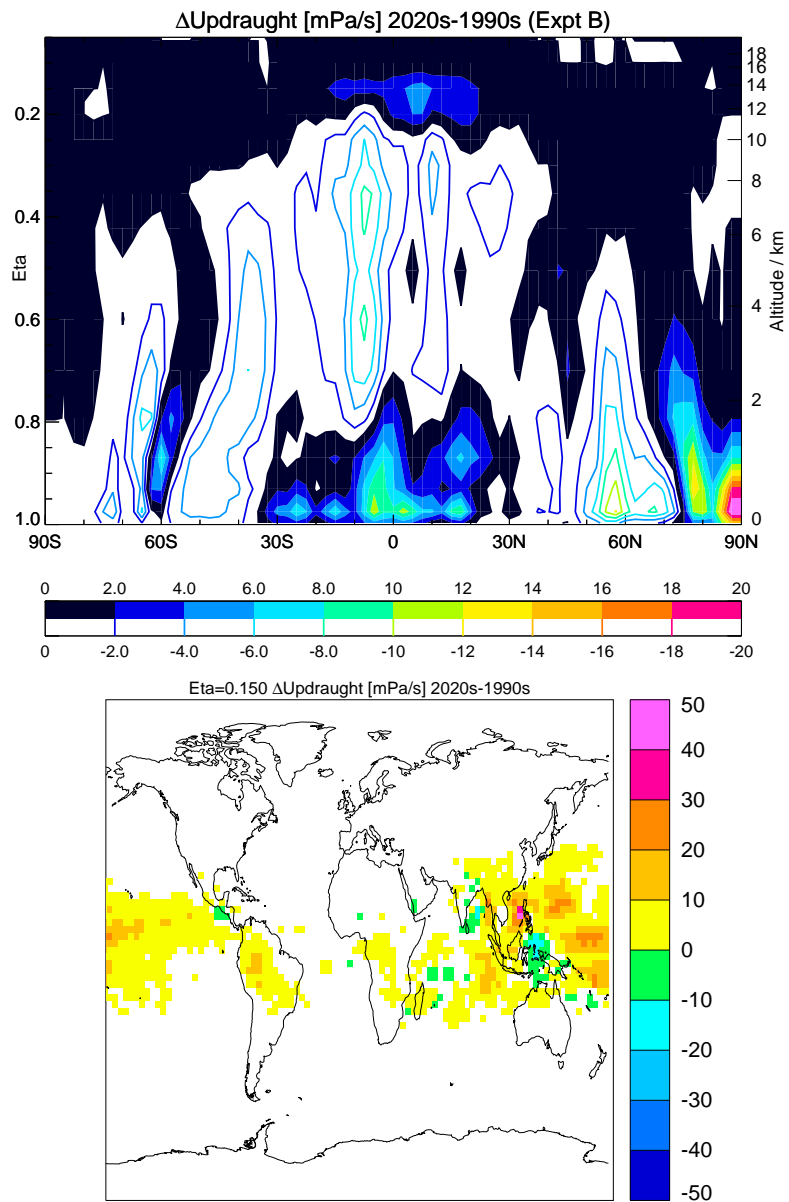


Figure 3 (a) Zonal mean change in convective updraught strength (mPa s^{-1}) due to climate change between the 1990s and 2020s; (b) change in convective updraught strength for the deepest convection (at ~ 150 hPa) for the same time period.

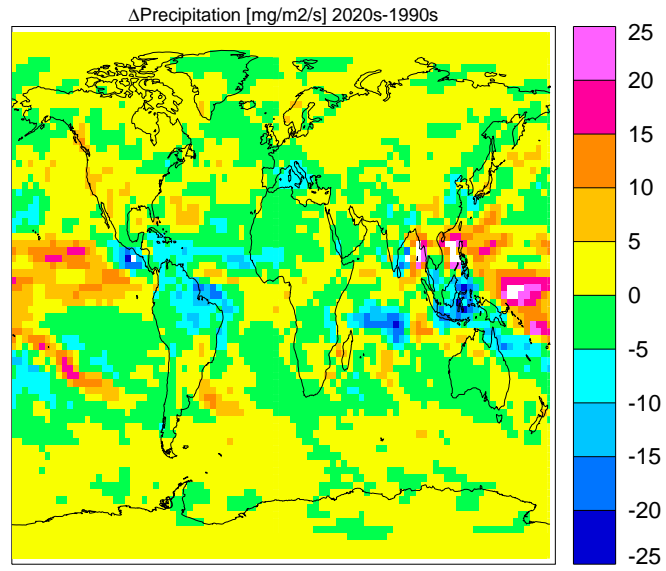


Figure 4 Change in total precipitation ($\text{mg m}^{-2} \text{s}^{-1}$) due to climate change between the 1990s and 2020s.

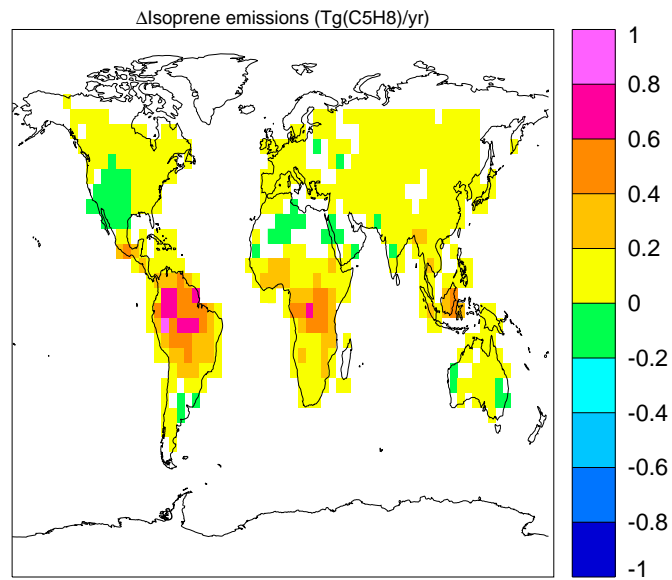


Figure 5 Change in isoprene emissions (Tg(C₅H₈) yr⁻¹) due to climate change between the 1990s and 2020s.

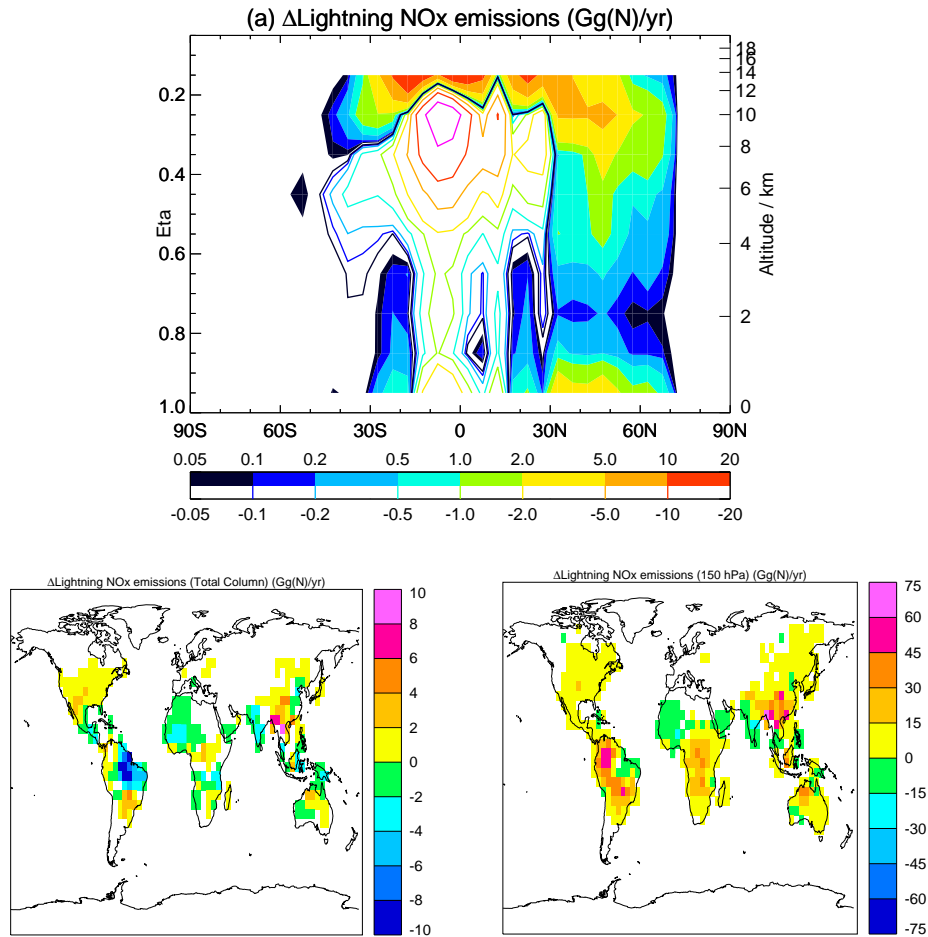


Figure 6 Change in lightning NO_x emissions (Gg(N) yr⁻¹) due to climate change between the 1990s and 2020s: (a) Zonal mean; (b) Column total; (c) 150 hPa level.

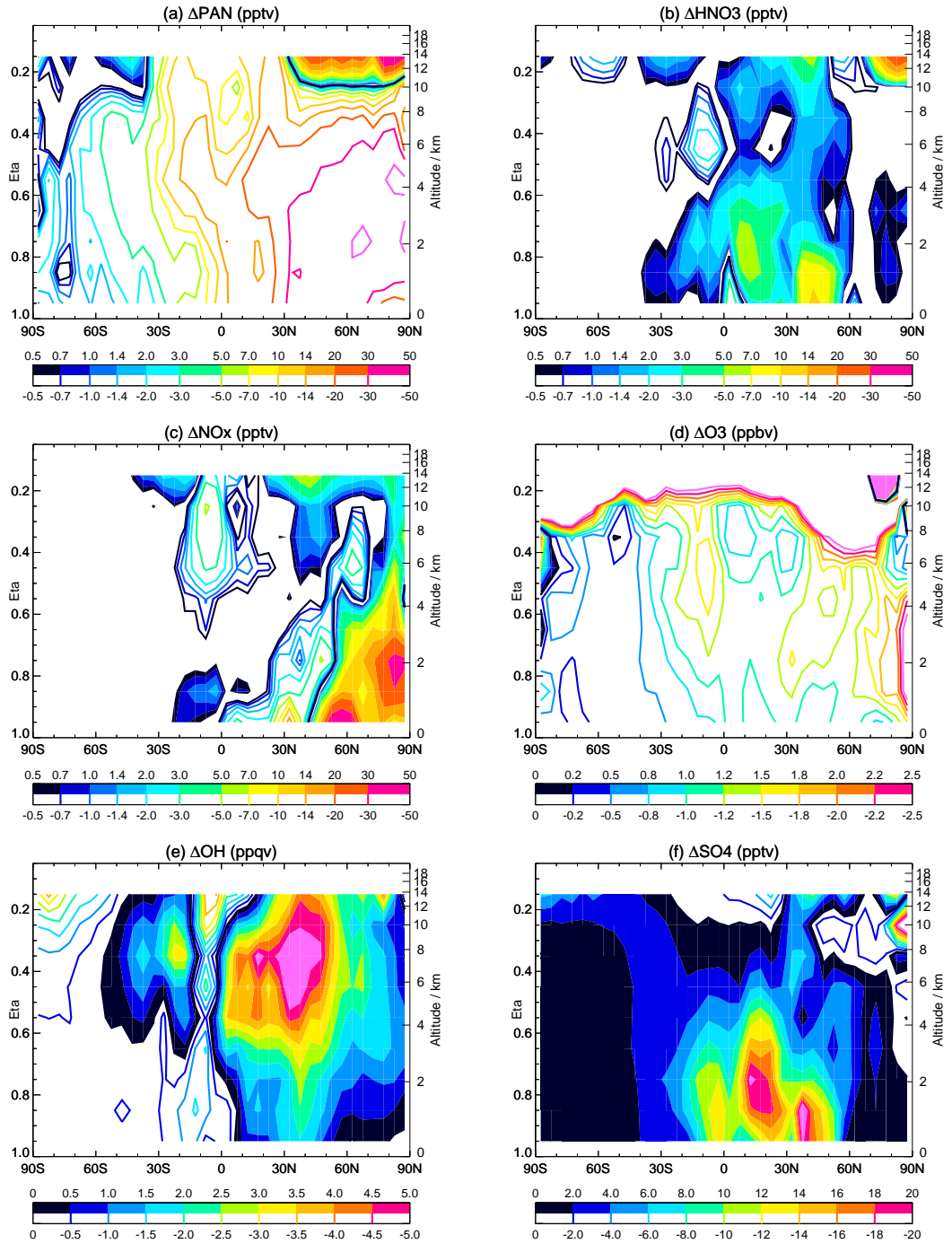


Figure 7 Zonal mean changes due to climate change between the 1990s and the 2020s: (a) PAN (pptv); (b) HNO₃ (pptv); (c) NO_x (pptv); (d) O₃ (ppbv); (e) OH (ppqv); (f) SO₄ (pptv).

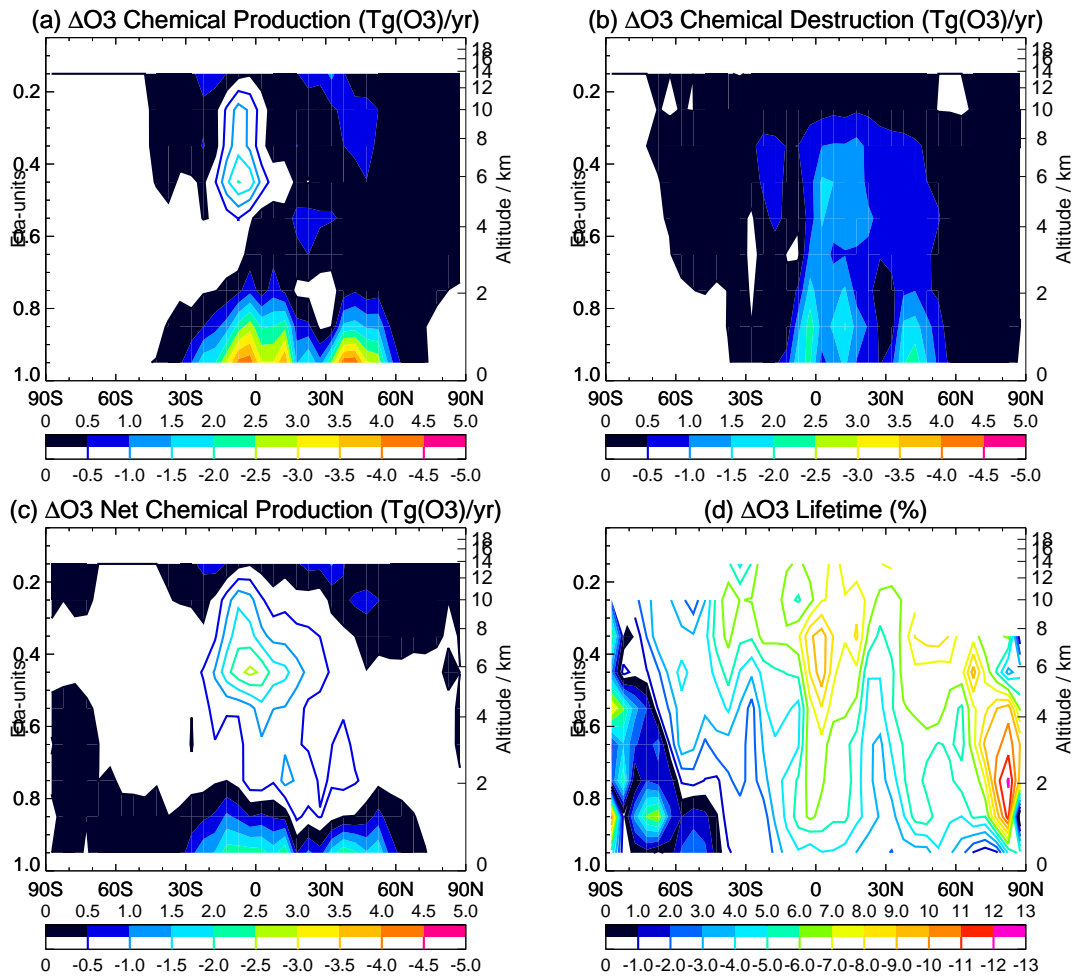


Figure 8 Zonal mean change, due to climate change between the 1990s and 2020s, in (a) O₃ chemical production; (b) O₃ chemical destruction; (c) O₃ net chemical production; (d) O₃ lifetime.

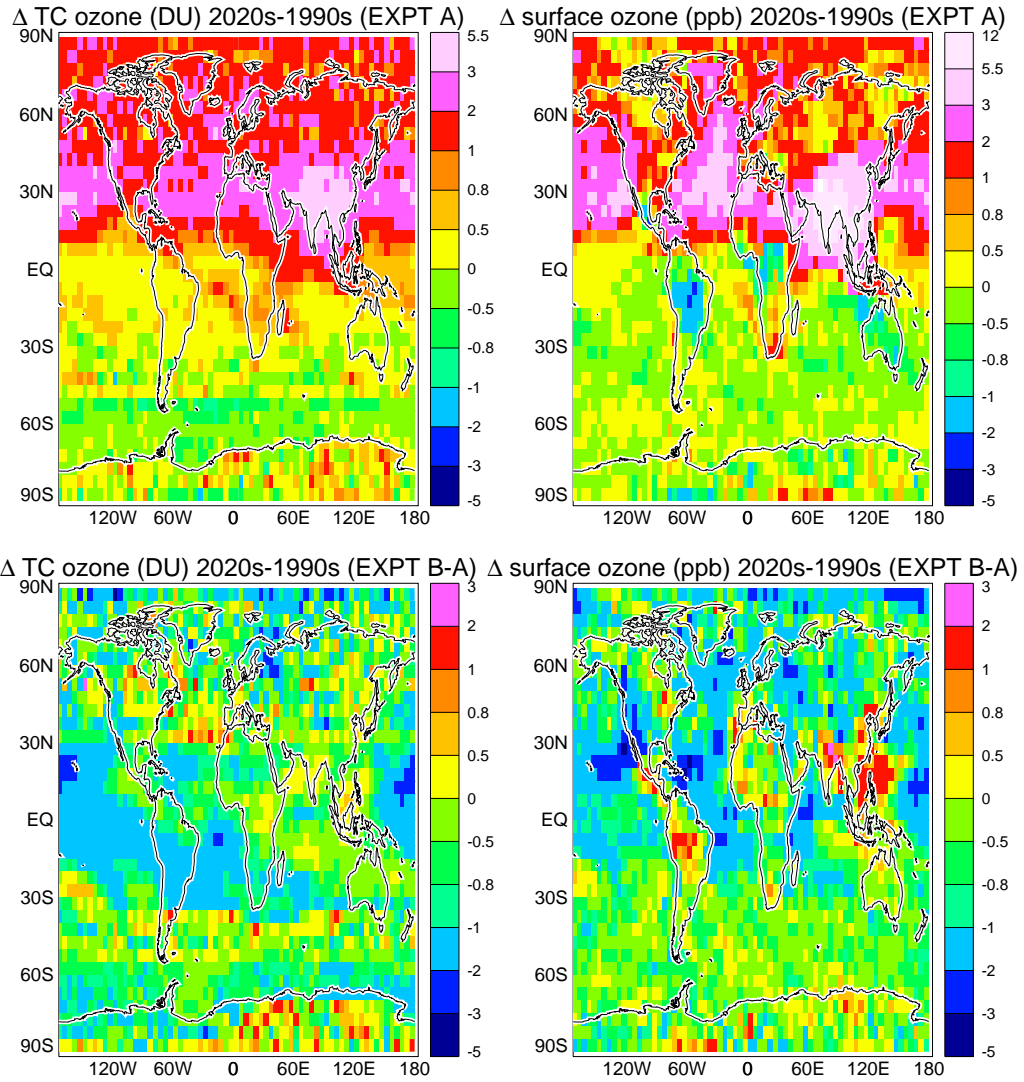


Figure 9 Change in tropospheric column O₃ (a, c) and surface O₃ (b, d) between the 1990s and 2020s, due to emissions (a, b); and climate change (c, d).

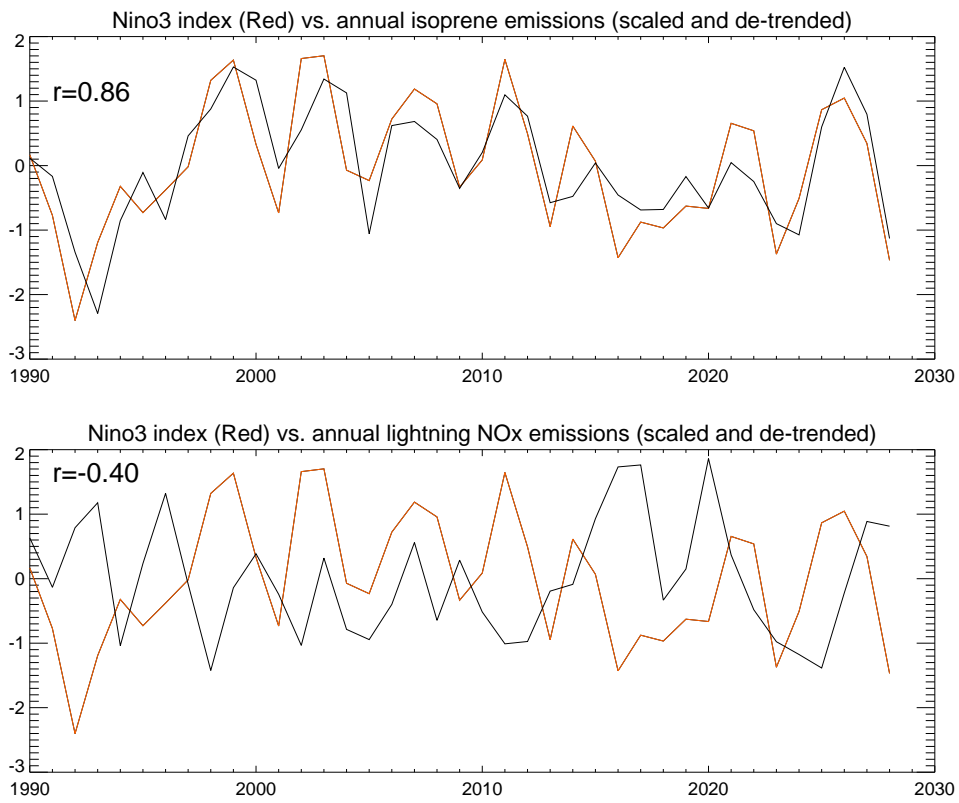


Figure 10 Niño-3 index and: (a) C_5H_8 emissions variability; (b) Lightning NO_x emissions variability.

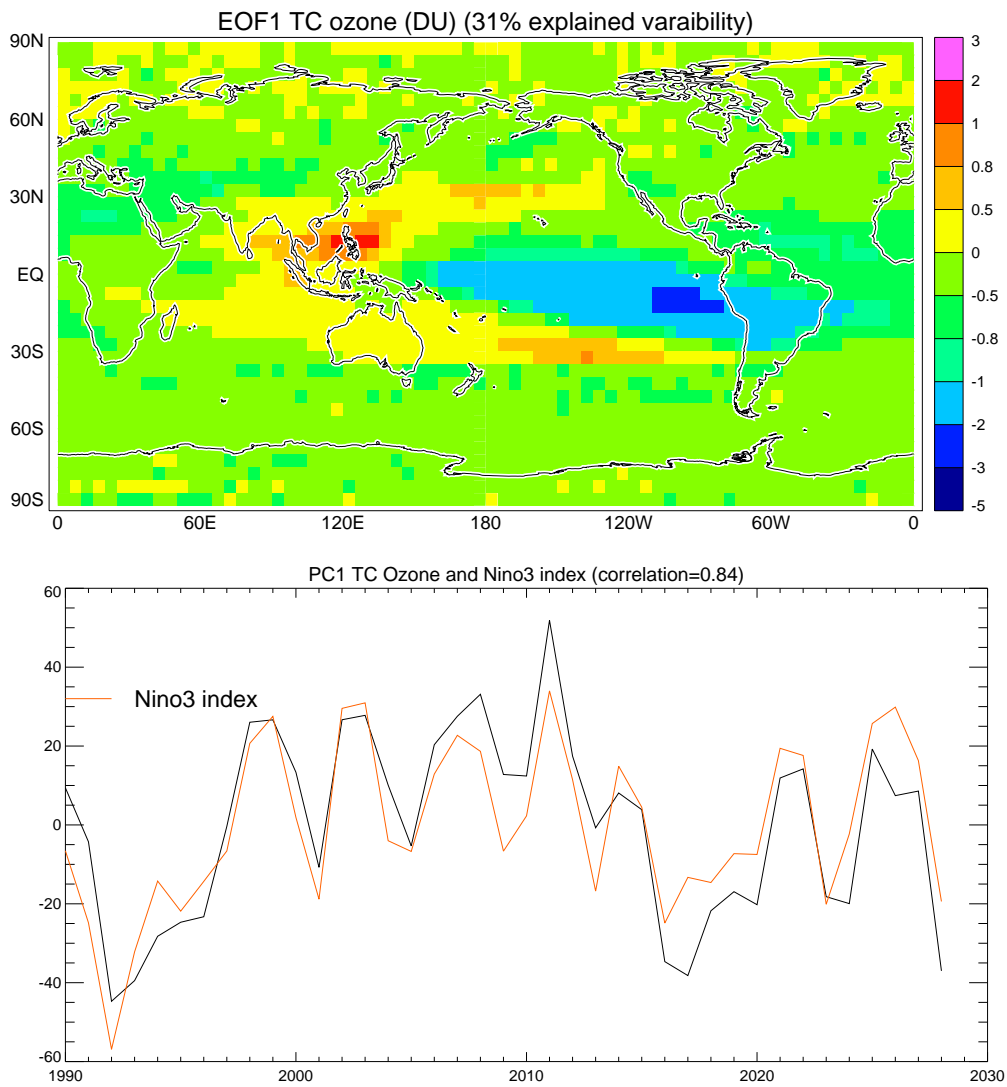


Figure 11 (a) First EOF for column O_3 , over the full length of experiment (B); (b) First principal component and the Niño-3 index, demonstrating that ENSO is the major mode of variability in total tropospheric column ozone.